Fabrication and Evaluation of Mesoporous Poly(vinyl alcohol)-Based Activated Carbon Fibers

ARTICLE *in* INDUSTRIAL & ENGINEERING CHEMISTRY RESEARCH · MARCH 2009

Impact Factor: 2.59 · DOI: 10.1021/ie8012852

6 AUTHORS, INCLUDING:

Shujuan Zhang
Nanjing University
78 PUBLICATIONS **1,697** CITATIONS
SEE PROFILE

Han-Qing Yu
University of Science and Technology of C…
508 PUBLICATIONS **11,036** CITATIONS
SEE PROFILE

Michael Lam
City University of Hong Kong
70 PUBLICATIONS **1,051** CITATIONS
SEE PROFILE

Article

Fabrication and Evaluation of Mesoporous Poly(vinyl alcohol)-Based Activated Carbon Fibers

Hui-Min Feng, Shu-Juan Zhang, Yong-Zhen Chen,
Yan-Wei Ding, Han-Qing Yu, and Michael Hon-Wah Lam

Ind. Eng. Chem. Res., **2009**, 48 (7), 3398-3402• DOI: 10.1021/ie8012852 • Publication Date (Web): 03 March 2009

Fabrication and Evaluation of Mesoporous Poly(vinyl alcohol)-Based Activated Carbon Fibers

Hui-Min Feng,[†,‡,§] Shu-Juan Zhang,[‡] Yong-Zhen Chen,[‡] Yan-Wei Ding,[||] Han-Qing Yu,*[,†,‡] and Michael Hon-Wah Lam[†,§]

Advanced Laboratory for Environmental Research & Technology, USTC-CityU, Suzhou, 215123, China, Department of Chemistry and Hefei National Laboratory for Physical Sciences at Microscale, University of Science & Technology of China, Hefei, 230026, China, and Department of Biology and Chemistry, City University of Hong Kong, Kowloon, Hong Kong

Poly(vinyl alcohol)- (PVA-) based activated carbon fibers (ACFs) with a high mesoporosity have been fabricated. The surface area and pore size distribution were fine-tuned by the careful control of the activation temperature and time. A mesopore volume fraction of 66% was obtained by activation at 1173 K for 120 min or 1273 K for 90 min. Raman spectroscopy revealed that more defect sites in the graphitic structure were found in samples with higher mesoporosity. Adsorption experiments demonstrated that the PVA-ACFs exhibited good adsorption capacities for both small-molecular-size iodine and the larger-size methylene blue, with adsorption capacities of up to 1934 and 709 mg/g, respectively. The adsorption kinetics of methylene blue on the PVA-ACFs was simulated by both a pseudo-second-order kinetic model and an intraparticle diffusion model. With an increase in mesoporosity, rate limitations on adsorption due to intraparticle diffusion were dramatically reduced. This resulted in an increase of up to a factor of 7 in the adsorption rate compared to that on microporous PVA-based ACFs.

1. Introduction

Adsorption is one of the most efficient methods for removing pollutants from water and air. As a type of carbonaceous adsorbent, activated carbon fibers (ACFs) have attracted considerable interest because of their numerous special features compared to conventional activated carbon.[1] For example, ACF materials can exist in a variety of forms, such as cloth, felt, and paper. Moreover, ACFs generally have narrower pore size distributions and allow greater accessibility of adsorbates to their micropores. These properties have endowed ACFs with high adsorption capacity for small-molecular-size pollutants, even at low concentrations. However, these features might not always be advantageous, especially when the ACFs are being used as electrodes/capacitor materials or as adsorbents for larger-molecular-size pollutants. In microporous carbon materials, adsorption occurs in pores with sizes about 1.7 times larger than the second widest dimension of the adsorbate molecules.[2,3] Therefore, for effective adsorption of larger-molecular-size pollutants, such as organic dyes, organophosphorus pesticides, and pharmaceuticals, sorbent materials with higher mesoporosity are required.[4−7] As reported previously, an increase in adsorbent mesoporosity enhances adsorption through the alleviation of pore blockage without compromising the adsorption capacity for small-size adsorbates.[8−11]

In this work, highly mesoporous poly(vinyl alcohol)- (PVA-) based ACFs (PVA-ACFs) were prepared. Our main objective was to regulate the surface area and pore volume fraction of these PVA-ACFs through the careful control of activation temperature and time. The textural properties and graphitic structure of the prepared ACFs were characterized by nitrogen adsorption and Raman spectroscopy. Boehm titration and determination of the point of zero charge (pH_{PZC}) were applied to characterize their surface chemical properties. The adsorption ability of the PVA-ACFs was evaluated by liquid adsorption of methylene blue (MB) and iodine.

2. Experimental Section

2.1. Reagents and Preparation of Mesoporous PVA-ACF. Wet-spun poly(vinyl alcohol) (PVA) filament yarn, purchased from Hunan Xiangwei Co., Hunan, China, was used as the precursor for ACF fabrication. The PVA filament yarn had a softening temperature of around 488−497 K. The salt residue from the coagulation bath in the yarn was about 15%. Diammonium phosphate (DAP) and MB were purchased from Sinopharm Chemical Reagent Co., Shanghai, China. All chemicals used in this study were of reagent grade. Detailed information about the preparation of the PVA-ACFs was described in our previous reports.[1,12] Briefly, a filament yarn of raw wet-spun PVA fibers of appropriate mass and length was first preoxidized in an air convection oven at 493 K for 2 h under a certain amount of tension supplied by springs. Then, the fibers were washed with water and thoroughly soaked in 5 wt % DAP solution. After being dried, the fibers were dehydrated at 523 K for 2 h in air and then carbonized at 573 K for 1 h in air. Finally, the fibers were activated at a specified temperature with static air for a predetermined period of time. Unless otherwise stated, the fabricated fibers are denoted as ACF-*T*-*t*, where *T* represents the activation temperature (in Kelvin) and *t* represents the activation time (in minutes).

2.2. Texture Structure. Nitrogen adsorption measurements were performed at 77.4 K using a volumetric adsorption analyzer (ASAP 2020M, Micromeritics Co., USA) at relative pressures from 10^{-7} to 1. All samples were degassed at 573 K for 10 h before analyses. Adsorption isotherms were used to analyze the surface areas and pore structures. The Brunauer−

* To whom correspondence should be addressed. Tel.: 86 551 3607592. Fax: 86 551 3607592. E-mail: hqyu@ustc.edu.cn.
† USTC-CityU.
‡ Department of Chemistry, University of Science & Technology of China.
§ City University of Hong Kong.
|| Hefei National Laboratory for Physical Sciences at Microscale, University of Science & Technology of China.

10.1021/ie8012852 CCC: $40.75
Published on Web 03/03/2009

Emmett−Teller (BET) equation was used to calculate the specific surface area, S_{BET}. The *t*-plot method was employed to calculate the surface area and volume of the micropores. The Barrett−Joyner−Halenda (BJH) method was employed to calculate the mesopore volume. Total pore volume was obtained from the single point adsorption at the relative pressure of 0.995. Pore size distributions were obtained by the density functional theory (DFT) method. Raman spectra were recorded using a Labram-010-Raman spectrometer with an argon-ion laser at an excitation wavelength of 488 nm.

2.3. Surface Chemistry Analysis. Boehm titration was used to determine the surface functional groups of the PVA-ACFs.[13] The following assumptions were made to distinguish the oxygen-containing complexes on the surface according to their acidity: NaOH neutralizes carboxylic, lactonic, and phenolic groups; Na_2CO_3 neutralizes carboxylic and lactonic groups; $NaHCO_3$ neutralizes carboxylic groups. Each basic solution (50 mL) was mixed with 0.05 g of PVA-ACFs and was shaken at 298 K for five days to reach equilibrium. A 20-mL portion of the basic supernatant was titrated with a 0.05 M hydrochloric acid solution using methyl orange as the indicator. Total basicity was determined by mixing 0.05 g of PVA-ACFs with 50 mL of a 0.05 M HCl solution. The final concentration of HCl was determined by titration with a 0.05 M NaOH solution.

The batch equilibrium technique was applied to determine pH_{PZC}.[14] A definite amount (50 mg) of PVA-ACFs was added to 20 mL of a 0.1 M potassium nitrate solution, used as an inert electrolyte, in a 50-mL stoppered conical flask. The initial pH of the solutions was adjusted from 1.5 to 10 by the addition of nitric acid and potassium hydroxide solutions. The mixtures were agitated at 298 K for 24 h to reach equilibrium. The final pH of the potassium nitrate solutions was measured and plotted against the initial pH. The value of pH_{PZC} was obtained from the plateau of constant pH.

2.4. Liquid-Phase Adsorption of MB and Iodine. Isothermal adsorption experiments were conducted in 100-mL iodine flasks, in which 50 mL of MB solutions of various initial concentrations ranging from 80 to 550 mg/L and 0.02 g of PVA-ACFs were placed. These flasks were kept in an isothermal shaker at 298 K for 3 days to reach equilibrium. Iodine number was determined according to the standard method specified by the American Society for Testing and Materials (ASTM).[15]

The adsorption kinetics was determined by dosing 0.05 g of the PVA-ACFs into 200 mL of a MB solution at a concentration of 230 mg/L. The mixture was magnetically stirred at 298 K. At appropriate time intervals, 1 mL of the MB solution was removed, diluted with distilled water to 25 mL, and analyzed by a UV−visible spectrometer (UV2450, Shimadzu Co., Japan) at 665 nm for the residual MB concentration.

3. Results and Discussion

3.1. Pore Structure. Nitrogen adsorption/desorption isotherms of the PVA-ACFs are shown in Figure 1. All of the isotherms show a sharp increase in adsorbed nitrogen at low relative pressures, indicating the presence of a microporous structure. Moreover, the appearance of hysteresis loops in the isotherms suggests the presence of mesopores.

The pore and surface structure parameters of all PVA-ACFs obtained from nitrogen adsorption analysis are summarized in Table 1. All of the PVA-ACFs exhibited large specific surface areas, S_{BET}. S_{BET} increased to 2640 m^2/g with increasing activation time and activation temperature. As the activation time increased, the micropore area decreased, but the external surface area increased. This suggests that, with increasing activation time, more pores opened on the fiber surface, and more micropores developed into meso- and/or macropores. This behavior was well reflected by the pore size distributions of the PVA-ACFs (Figure 2).

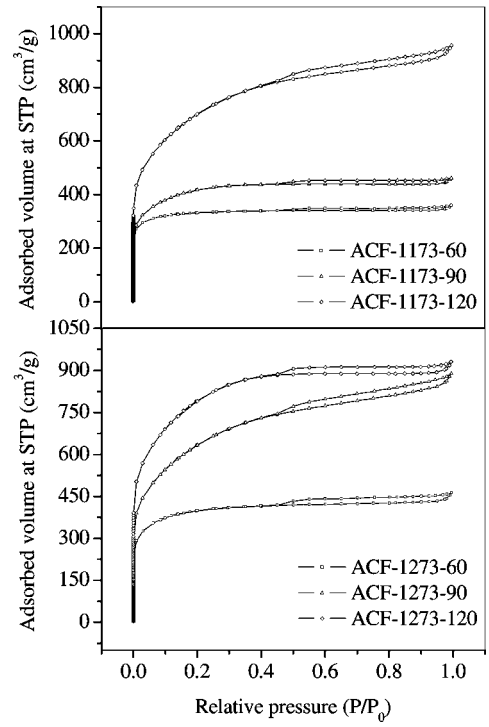

Figure 1. N_2 adsorption isotherms of PVA-ACFs.

Table 1. Characteristics of the PVA-ACFs

activation temperature (K):	1173			1273		
activation time (min):	60	90	120	60	90	120
yield (%)	26.0	18.9	16.2	20.4	15.5	12.6
S_{BET} (m^2/g)	1010	1322	2371	1241	2158	2640
micropore area (m^2/g)	808	670	481	794	400	703
micropore volume (cm^3/g)	0.423	0.352	0.246	0.417	0.213	0.365
mesopore volume (cm^3/g)	0.086	0.221	0.941	0.215	0.903	0.726
total pore volume (cm^3/g)	0.556	0.714	1.480	0.716	1.376	1.441
iodine number (mg/g)	1626	1806	1845	1849	1916	1934
MB adsorption capacity (mg/g)	211	457	519	529	588	709

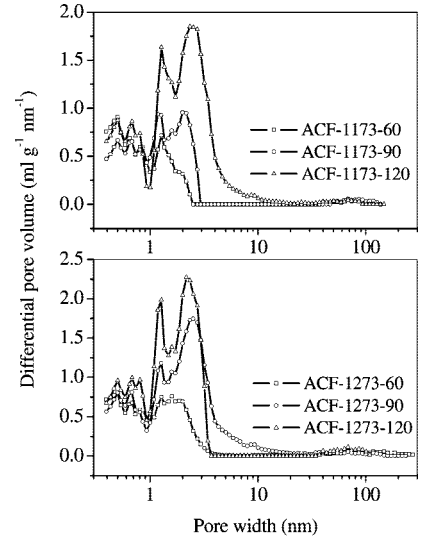

Figure 2. Pore size distributions calculated by the DFT method from N_2 adsorption isotherms at 77 K on PVA-ACFs.

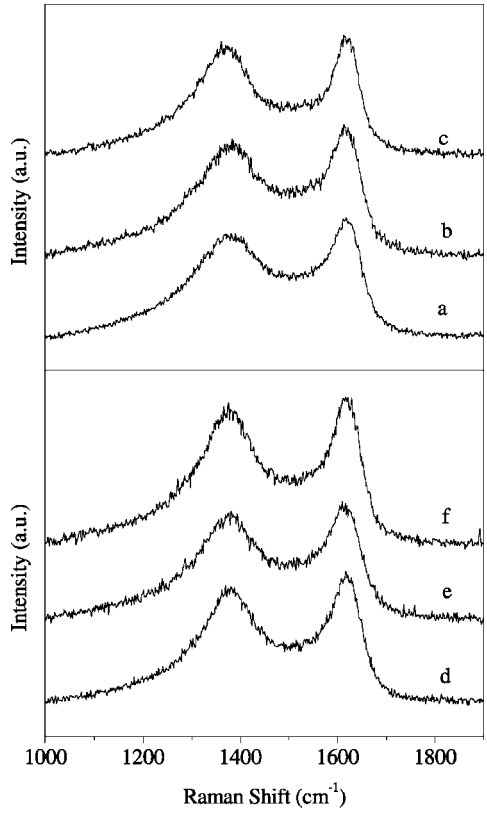

Figure 3. Raman spectra of the PVA-ACFs: (a) ACF-1173-60, (b) ACF-1173-90, (c) ACF-1173-120, (d) ACF-1273-60, (e) ACF-1273-90, (f) ACF-1273-120.

As seen in Figure 2, the PVA-ACFs activated at 1173 K showed a regular evolution of pore width: the longer the activation time, the wider the pore size distribution, and the larger the mesopore volume fraction. ACF-1173-60 was predominated by micropores with a pore size distribution centered at 1.3 nm; its mesopore fraction was 15%. In contrast, ACF-1173-120 was highly mesoporous in that, in addition to the peak in the micropore range (1.3 nm), another peak in the mesopore range (2.3 nm) was observed. Its mesopore fraction reached 64%. Interesting results were observed for ACFs activated at 1273 K. Similar to ACF-1173-60, ACF-1273-60 was also micropore-dominated, but with a higher volume fraction of mesopores. However, the pore size distribution shrank when the activation time was over 90 min. The mesopore fraction decreased from 66% to 50%, and the mesopore peak in the pore size distribution decreased from 2.5 to 2.2 nm when the activation time was increased from 90 to 120 min. In other words, the mesopore fraction in the PVA-ACFs did not increase in linearly with activation time. This might be due to the development of mesopores to macropores and the collapse of those macropores into caves or channels upon prolonged activation. As the macropores collapsed, new micropores were generated, resulting in a shrinking of the pore size distribution and a decrease in the mesopore fraction. With the fabrication conditions developed in this work, mesoporous PVA-ACFs with a mesopore fraction of up to 66% can be obtained. The highest mesopore fraction was achieved by activation at 1173 K for 120 min or at 1273 K for 90 min.

3.2. Graphitic Structure. As shown in Figure 3, two characteristic bands were observed in the Raman spectra of the PVA-ACFs at around 1617 and 1381 cm^{-1}. The former is denoted as the G-band, which originated from the E_{2g} vibration mode of an ordered graphitic structure, whereas the latter is denoted as the D-band and is associated with defect structures and disorder.[16−18] There was no difference in the band positions among the spectra of the various PVA-ACFs, but the D-to-G band intensity ratio, $I(D)/I(G)$, varied with the activation temperature and activation time. For PVA-ACF samples activated at 1173 K, $I(D)/I(G)$ increased from 0.88 to 0.91 and then to 0.94 with increasing activation time from 60 to 120 min. The corresponding $I(D)/I(G)$ values for the PVA-ACFs activated at 1273 K were 0.91, 0.93, and 0.96. These $I(D)/I(G)$ values suggest that a higher degree of surface disorder/defect was obtained in PVA-ACFs that were activated at a higher temperature or for a longer duration. This might be due to the fact that a higher activation temperature and a longer activation time enhanced the reaction of carbon atoms in the fibers with the oxidizing gas. This resulted in the generation of more pores, which led to the formation of more defects and disordered structures.

Table 2. Surface Chemical Parameters of the PVA-ACFs

	surface functional groups (mequiv/g)					
sample	carboxylic	lactonic	phenolic	total acidic	basic	pH_{PZC}
ACF-1173-60	0.30	0.64	0.34	1.28	0.24	6.47
ACF-1173-90	0.02	0.59	0.49	1.10	0.45	7.06
ACF-1173-120	0.11	0.44	0.29	0.41	0.58	7.15
ACF-1273-60	0	0.41	0.66	1.05	0.41	6.98
ACF-1273-90	0.08	0.31	0.44	0.84	0.56	7.35
ACF-1273-120	0.04	0.36	0.12	0.52	0.64	7.66

3.3. Surface Chemical Properties. Table 2 lists the Boehm titration results. The number of total acidic group decreased significantly with increasing activation time and temperature. The number of basic groups, on the other hand, increased with increasing activation time and temperature. The pH_{PZC} values of the PVA-ACFs were in a range of 6.47−7.66. This is consistent with the change of acidic and basic surface functional groups.

3.4. Batch Equilibrium Adsorption. The adsorption capacities of the PVA-ACFs fabricated in this work were evaluated using the two universal indicators, iodine and MB, serving as model adsorbates. As shown in Table 1, the iodine numbers of all of the PVA-ACFs were in the range of 1626−1934 mg/g. Among the samples, there were no significant differences, except for microporous ACF-1173-60. In contrast, the adsorption behaviors with respect to MB of the PVA-ACFs obtained at different activation temperatures and durations were quite different (Figure 4). The adsorption isotherms of the various PVA-ACFs for MB were well described by the Langmuir equation with correlation coefficients higher than 0.999. The maximum adsorption capacity (q_m) values obtained are reported in Table 1. The q_m of MB was proportional to the mesopore fraction of the PVA-ACFs. The highest adsorption capacity for MB was 709 mg/g. This is much higher than the values for ACFs obtained by other preparation methods, e.g., reactivation.[2]

3.5. Adsorption Kinetics of MB. In addition to adsorption capacity, adsorption kinetics is another important factor to consider in the application of adsorbents. All of the kinetic adsorption plots for MB on PVA-ACFs show a sharp initial stage, but the length of the equilibrium time is a function of the mesopore volume fraction. An increase in the mesopore fraction shortened the time for adsorption equilibrium. The adsorption rate constants (Table 3) were obtained with the pseudo-second-order equation

$$\frac{t}{q_t} = \frac{1}{k_2 q_e^{\,2}} + \frac{t}{q_e} \qquad (1)$$

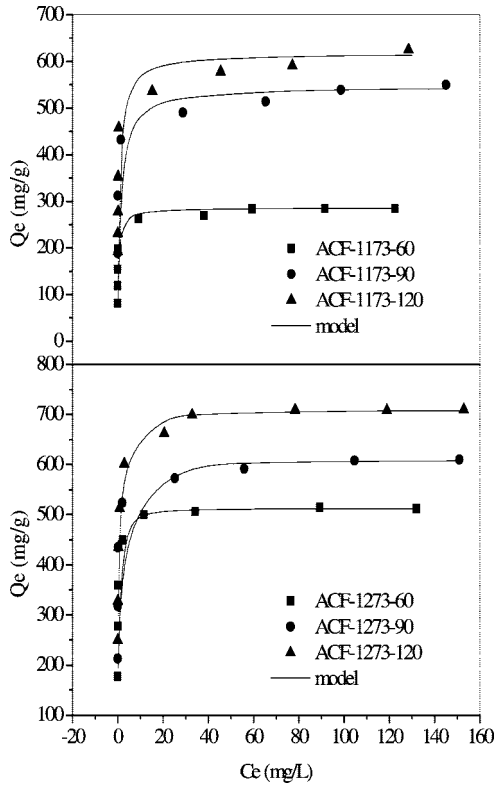

Figure 4. Adsorption isotherms of MB on PVA-ACFs. Points, experimental data; curves, Langmuir modeling.

Table 3. Kinetic Parameters for the Adsorption of MB onto PVA-ACFs

activation temperature (K):	1173			1273		
activation time (min):	60	90	120	60	90	120
$k_2 \times 10^{-4}$ [g/(mg min)]	0.7	1.6	3.6	1.3	4.2	4.8
k_{id} [mg/(g min$^{0.5}$)]	30	111	132	90	200	356

where q_t (mg/g) is the amount of MB adsorbed per gram of adsorbent over a time period of t (min), q_e (mg/g) is the equilibrium saturated adsorption capacity of MB, and k_2 [g/(mg min)] is the pseudo-second-order adsorption rate constant. With increasing mesopore volume fraction, the rate constant increased dramatically.

The prediction of the rate-limiting step is an important aspect to consider in a sorption process.[19] The parameter k_2 in the pseudo-second-order kinetic model is an overall rate constant. It cannot be used to distinguish different adsorption mechanisms. Therefore, an intraparticle diffusion model must be employed to identify the mechanism involved in the adsorption process. If a plot of q versus $t^{1/2}$ produces a straight line, the sorption process is controlled by intraparticle diffusion only. If the data exhibit multilinear plots, then the sorption process is influenced by two or more steps.[20,21]

Figure 5 shows a multilinear fitting of the adsorption kinetics to the intraparticle diffusion model. This multilinearity indicates the occurrence of two or more "steps" in the adsorption process. The first, sharper portion indicates a boundary-layer-diffusion effect or an external-mass-transfer effect. The slope of the second linear portion of the plot was used to obtain the intraparticle diffusion parameter, k_{id}. The intercept of the second portion reflects the boundary-layer effect. The larger the intercept, the greater the contribution of external mass transfer in the rate-limiting step.[19,21] The rate of intraparticle diffusion is much lower than the rate of external mass transfer. A higher contribution of external mass transfer leads to a higher adsorption rate constant. This was supported by the k_2 values. The third portion is the final equilibrium stage. Within the given contact time, no equilibrium stage was observed in the adsorption of MB onto microporous PVA-ACFs, whereas an equilibrium stage was observed in the adsorption of MB onto mesoporous PVA-ACFs. This demonstrates that mesopores in the PVA-ACFs can significantly enhance the rate of MB adsorption.

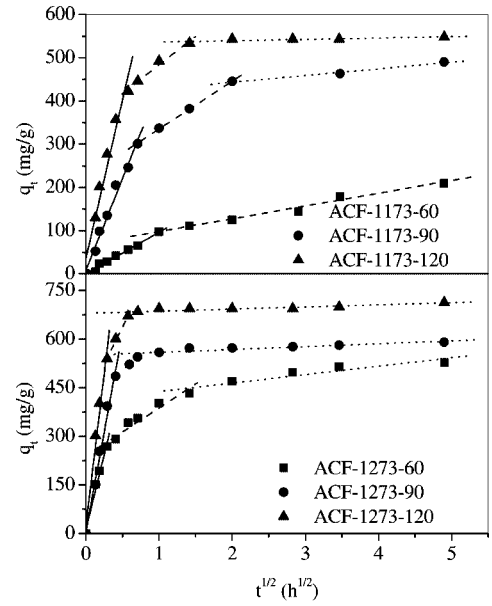

Figure 5. Fractional uptake curve for MB onto PVA-ACFs. Points, experimental data; curves, intraparticle diffusion modeling.

4. Conclusions

A set of highly mesoporous PVA-ACFs was fabricated. The textural properties of the ACFs, including surface area and pore volume distribution, were fine-tuned by the careful control of the activation temperature and activation time. A mesopore volume fraction of 66% was obtained with activation at 1173 K for 120 min or at 1273 K for 90 min. Adsorption experiments demonstrated that these PVA-ACFs exhibit good adsorption capacities for both small-molecular-size iodine and larger-size MB, with adsorption capacities of up to 1934 and 709 mg/g, respectively. With an increase in mesoporosity, the extent of intraparticle-diffusion limitations on the adsorption rate was dramatically reduced. An increase of up to a factor of 7 in the adsorption rate can be obtained. The surface chemical properties of the PVA-ACFs, including surface functional groups and pH_{pzc}, were also characterized. The surface chemical properties were also fine-tuned by controlling the activation conditions. These PVA-ACFs are potentially useful in the selective adsorption of pollutants.

Acknowledgment

The authors thank the Natural Science Foundation of China (50625825) for partial support of this study.

Literature Cited

(1) Zhang, S. J.; Yu, H. Q.; Feng, H. M. PVA-based Activated Carbon Fibers with Lotus Root-like Axially Porous Structure. *Carbon* **2006**, *44*, 2059.

(2) Kasaoka, S.; Sakata, Y.; Tanaka, E.; Naito, R. Designation of Molecular Sieve Carbon. Studies on the Adsorption of Various Dyes in the Liquid Phase. *Int. Chem. Eng.* **1989**, *29*, 7344.

(3) Yuan, R. S.; Guan, R. B.; Zheng, J. T. Effect of the Pore Size of TiO_2-Loaded Activated Carbon Fiber on Its Photocatalytic Activity. *Scr. Mater.* **2005**, *52*, 1329.

(4) Tseng, R. L.; Tseng, S. K. Pore Structure and Adsorption Performance of the KOH-Activated Carbons Prepared from Corncob. *J. Colloid Interface Sci.* **2005**, *287*, 428.

(5) Yang, X. Y.; Al-Duri, B. Kinetic Modeling of Liquid-Phase Adsorption of Reactive Dyes on Activated Carbon. *J. Colloid Interface Sci.* **2005**, *287*, 25.

(6) Malik, P. K. Use of Activated Carbons Prepared from Sawdust and Rice Husk for Adsorption of Acid Dyes: A Case Study of Acid Yellow 36. *Dyes Pigment* **2003**, *56*, 239.

(7) Macedo, J. D.; da Costa, N. B.; Almeida, L. E.; Vieira, E. F. D.; Cestari, A. R.; Gimenez, I. D. Kinetic and Calorimetric Study of the Adsorption of Dyes on Mesoporous Activated Carbon Prepared from Coconut Coir Dust. *J. Colloid Interface Sci.* **2006**, *298*, 515.

(8) Hsieh, C. T.; Teng, H. S. Influence of Mesopore Volume and Adsorbate Size on Adsorption Capacities of Activated Carbons in Aqueous Solutions. *Carbon* **2000**, *38*, 863.

(9) Abe, I.; Fukuhara, T.; Kawasaki, N.; Hitomi, M.; Kera, Y. Characteristics of Cyclodextrin Adsorption onto Activated Carbons. *J. Colloid Interface Sci.* **2000**, *229*, 615.

(10) Li, Q. L.; Snoeyink, V. L.; Marinas, B. J.; Campos, C. Elucidating Competitive Adsorption Mechanisms of Atrazine and NOM Using Model Compounds. *Water Res.* **2003**, *37*, 773.

(11) Li, Q. L.; Snoeyink, V. L.; Marinas, B. J.; Campos, C. Pore Blockage Effect of NOM on Atrazine Adsorption Kinetics of PAC: The Roles of PAC Pore Size Distribution and NOM Molecular Weight. *Water Res.* **2003**, *37*, 4863.

(12) Zhang, S. J.; Feng, H. M.; Wang, J. P.; Yu, H, Q. Structure Evolution and Optimization in the Fabrication of PVA-Based Activated Carbon Fibers. *J. Colloid Interface Sci.* **2008**, *321*, 96.

(13) Boehm, H. P. Some Aspects of the Surface Chemistry of Carbon Blacks and Other Carbons. *Carbon* **1994**, *32*, 759.

(14) Babic, B. M.; Milonjic, S. K.; Polovina, M. J.; Kaludierovic, B. V. Point of Zero Charge and Intrinsic Equilibrium Constants of Activated Carbon Cloth. *Carbon* **1999**, *37*, 477.

(15) Standard Test Method for Determination of Iodine Number of Activated Carbon. D4607-94; ASTM International: West Conshohocken, PA, 1999.

(16) Lei, S.; Miyamoto, J.; Kanoh, H.; Nakahigashi, Y.; Kaneko, K. Enhancement of the Methylene Blue Adsorption Rate for Ultramicroporous Carbon Fiber by Addition of Mesopores. *Carbon* **2006**, *44*, 1884.

(17) Lespade, P.; Al-Jishi, R.; Dresselhaus, M. S. Model for Raman Scattering from Incompletely Graphitized Carbons. *Carbon* **1982**, *20*, 427.

(18) Jia, J. F.; Wang, Y.; Tanabe, E.; Shishido, T.; Takehira, K. Carbon Fibers Prepared by Pyrolysis of Methane over Ni/MCM-41 Catalyst. *Microporous Mesoporous Mater.* **2003**, *57*, 283.

(19) Kalavathy, M. H.; Karthikeyan, T.; Rajgopal, S.; Miranda, L. R. Kinetic and Isotherm Studies of Cu(II) Adsorption onto H_3PO_4-Activated Rubber Wood Sawdust. *J. Colloid Interface Sci.* **2005**, *292*, 354.

(20) Wu, F. C.; Tseng, R. L.; Juang, R. S. Comparisons of Porous and Adsorption Properties of Carbons Activated by Steam and KOH. *J. Colloid Interface Sci.* **2005**, *283*, 49.

(21) Vadivelan, V.; Kumar, K. V. Equilibrium, Kinetics, Mechanism, and Process Design for the Sorption of Methylene Blue onto Rice Husk. *J. Colloid Interface Sci.* **2005**, *286*, 90.

Received for review August 24, 2008
Revised manuscript received January 22, 2009
Accepted January 23, 2009

IE8012852